

**LAYERED SILICATES (SODIUM MONTMORILLONITE)
BASED ELASTOMER NANOCOMPOSITES**

Tassawuth Pojanavaraphan

A Dissertation Submitted in Partial Fulfilment of the Requirements
for the Degree of Doctor of Philosophy
The Petroleum and Petrochemical College, Chulalongkorn University
in Academic Partnership with
The University of Michigan, The University of Oklahoma,
and Case Western Reserve University

2010

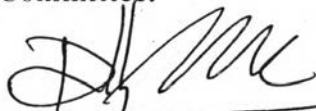
I 28375464

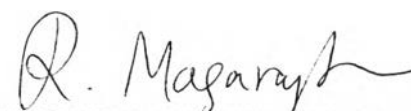
Thesis Title: Layered silicates (sodium montmorillonite) based elastomer nanocomposites
By: Tassawuth Pojanavaraphan
Program: Polymer Science
Thesis Advisors: Assoc. Prof. Rathanawan Magaraphan
Prof. David A. Schiraldi

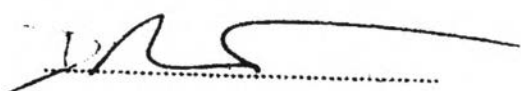
Accepted by The Petroleum and Petrochemical College, Chulalongkorn University, in partial fulfilment of the requirements for the Degree of Doctor of Philosophy.

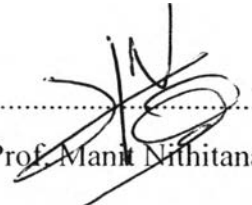

..... College Dean
(Asst. Prof. Pomthong Malakul)


Thesis Committee:


.....
(Asst. Prof. Pomthong Malakul)


.....
(Assoc. Prof. Rathanawan Magaraphan)


.....
(Prof. David A. Schiraldi)


.....
(Asst. Prof. Manit Nithitanakul)


.....
(Dr. Orasa Onjun)

ABSTRACT

4982004063: Polymer Science Program

Tassawuth Pojanavaraphan: Layered silicates (sodium montmorillonite) based elastomer nanocomposites.

Thesis Advisors: Assoc. Prof. Rathanawan Magaraphan (*Thai Advisor*) and Prof. David A. Schiraldi (*Overseas Advisor*)

Keywords: Admicellar polymerization/ Clay aerogel/ Freeze-drying/ Natural Rubber/ Polypyrrole

Two novel techniques known as freeze-drying and electrolytic admicellar polymerization were herein conducted for fabricating the natural rubber (NR)-based composites. These approaches were considered to be ideal for creating various types of NR-based materials that stood out as good candidates for a wide variety of applications ranging from thermal insulation till actuator or sensor. By utilizing a freeze-drying, the granular appearance of pristine clay (sodium montmorillonite, Na⁺-MMT) was converted into a monolith 'house of cards' structure with a bulk density of typically 0.05 g cm⁻³. This was originated from the parallel alignment of clay bundles along the ice crystal through electrostatic interactions between edge and face (EF) of clay particles. As the neat clay aerogel was relatively fragile, natural rubber (NR) latex was then introduced, followed by the cross-linking process to increase the materials structural integrity without harming the bulk density and microstructure. This reinforcement was illustrated by a good connectivity between each single sheet through a web of the NR matrix, thus promoting the load transfer under the applied stress. Further, to enable the production of semiconducting materials based on NR and Na⁺-MMT, polypyrrole (PPy) was introduced and served as a path for an effective charge transportation (electron hopping). This was accomplished by conducting an electrolytic admicellar polymerization of the corresponding aqueous solution. It was seen that the morphological characteristics as well as mass fractions of both PPy and Na⁺-MMT were crucial in determining the composites electrical conductivity, mechanical, and thermal performances.

บทคัดย่อ

ทศสวุทธิ์ พจนาวราพันธุ์ : ชื่อหัวข้อวิทยานิพนธ์ (ภาษาไทย) นาโนคอมพอสิตของ ยางอีลาสโตเมอร์ และ มอลต์มอลิไลไนต์ (Layered silicates (sodium montmorillonite) based elastomer nanocomposites) อาจารย์ที่ปรึกษา : รศ.ดร. รัตนาวรรณ มกรพันธุ์ และ ศ.ดร. เดวิด เอ. เฉอรวาดี 237 หน้า

ในรายงานวิจัยนี้ สองวิธีการใหม่ที่มีชื่อว่ากระบวนการแช่แข็งแห้งและกระบวนการแอคไมเซลลาพอลิเมอร์ไรเซชันแบบอิเล็กโทรไลต์ได้นำไปใช้สำหรับการผลิตวัสดุคอมพอสิตของยางธรรมชาติ ซึ่งมีคุณสมบัติที่แตกต่างกันและเนื่องด้วยเหตุนี้ วัสดุดังกล่าวอาจจะถูกนำไปประยุกต์ใช้กับหลายๆด้าน อาทิเช่น ด้านความเป็นฉนวนทางความร้อนจนถึงสมบัติด้านความต้านทานต่อคลื่นแม่เหล็กไฟฟ้า โดยที่วิธีการแช่แข็งแห้งนั้นสามารถทำให้เกิดการเปลี่ยนแปลงรูปพรรณสัณฐานวิทยาของเคลย์จากแบบอนุภาคในระดับไมครอนสู่โครงสร้างที่มีการจัดเรียงตัวเป็นแบบแผ่น ซึ่งมีน้ำหนักที่เบากว่าน้ำหนักของอนุภาคเคลย์ดั้งเดิม โครงสร้างสัณฐานวิทยาแบบลามลาร์เกิดขึ้นได้จากการจัดเรียงตัวใหม่ของแผ่นเคลย์โดยผ่านทางแรงดึงดูดแบบไฟฟ้าสถิตระหว่างพื้นผิวหน้าและด้านข้างของอนุภาคเคลย์ อย่างไรก็ตาม เนื่องด้วยความเปราะบางของเคลย์แอโรเจลนี้ เคลย์แอโรเจลจึงถูกผสมเข้ากับน้ำยางธรรมชาติรวมทั้งถึงขั้นตอนของกระบวนการเชื่อมขวาง เพื่อก่อให้เกิดการพัฒนาทางด้านความแข็งแรงเชิงกลของวัสดุคอมพอสิตที่ถูกจัดเตรียมขึ้น โดยปราศจากการเปลี่ยนแปลงทางด้านความหนาแน่นและรูปพรรณสัณฐานวิทยา การเสริมแรงชนิดนี้สามารถถูกอธิบายได้ด้วยการเชื่อมต่อที่พอเหมาะระหว่างแผ่นลามลาร์ โดยมียางธรรมชาติเป็นตัวประสานซึ่งส่งผลให้มีการถ่ายเทความเค้นได้เป็นอย่างดี นอกจากนี้เพื่อที่จะทำการผลิตวัสดุกึ่งนำไฟฟ้าจากยางธรรมชาติ พอลิไพโรลจึงนำมาใช้เป็นส่วนหนึ่งของระบบเพื่อที่จะก่อให้เกิดช่องทางสำหรับการเคลื่อนที่หรือการเดินทางของประจุไฟฟ้า หรือที่เรียกว่าอิเล็กตรอน ซึ่งจะนำไปสู่การนำไฟฟ้าในที่สุด ด้วยเหตุนี้กระบวนการที่เรียกว่า “แอคไมเซลลาพอลิเมอร์ไรเซชันแบบอิเล็กโทรไลต์” จึงถูกเลือกใช้ในการสังเคราะห์วัสดุกึ่งนำไฟฟ้าชนิดนี้ และมันถูกพบว่าโครงสร้างสัณฐานวิทยาเช่นเดียวกับกับสัดส่วนมวลของพอลิไพโรลและมอลต์มอลิไลไนต์มีความสำคัญอย่างยิ่งต่อสมบัติทางด้านไฟฟ้า สมบัติเชิงกล และ สมบัติทางความร้อนของวัสดุคอมพอสิตที่ถูกจัดเตรียมขึ้น

ACKNOWLEDGEMENTS

The completion of this dissertation would not be possible without sincerely acknowledging Assoc. Prof. Rathanawan Magaraphan, my research advisor, for providing me with exceptional guidance, pure inspiration, encouragement, freedom in every aspect, as well as an opportunity to experience the quality research. It has been a pleasure working with her for the past five years.

I would like to extend my gratitude to Prof. David A. Schiraldi, Chair of the Macromolecular Science and Engineering Department, Case Western Reserve University (CWRU) for his wonderful guidance and for being a truly nice overseas advisor during my period of stay (nine months) at CWRU. It has been a pleasure working with him as well.

I am grateful for the financial support provided by the Thailand Research Fund through the Royal Golden Jubilee Ph.D. Program, Polymer Processing and Polymer Nanomaterials Unit, the Rachadapisek Sompoch Endowment, the Asian Development Bank (ADB), the Petroleum and Petrochemical College (PPC), and the National Center of Excellence for Petroleum, Petrochemicals, and Advanced Materials, Thailand.

I would like to express my appreciation to all the PPC faculties for providing the invaluable fundamental knowledge not only in the polymer science but also in the petroleum and petrochemical fields, and to all PPC staffs for their great contributions throughout my study for the past five years.

Special thanks go to all the PPC and CWRU friends for their great friendship, creative guidance, helpfulness, and encouragement.

Lastly, all of these achievements would be worthless if there was no understanding and emotional support from my parents and brothers, whom I dedicate this dissertation to.

TABLE OF CONTENTS

	PAGE
Title Page	i
Abstract (in English)	iii
Abstract (in Thai)	iv
Acknowledgements	v
Table of Contents	vi
List of Tables	x
List of Figures	xiii
Abbreviations	xxi
List of Symbols	xxiv
CHAPTER	
I INTRODUCTION	1
II THEORETICAL BACKGROUND AND LITERATURE REVIEW	4
2.1 Clay Chemistry	4
2.2 Elastomer Nanocomposites	14
2.3 Electrically Conducting Polymers (CPs)	22
2.4 Admicellar Polymerization	28
III EXPERIMENTAL	36
3.1 Materials	36
3.2 Methodology	36
IV PREVULCANIZED NATURAL RUBBER LATEX/CLAY AEROGEL NANOCOMPOSITES	48
4.1 Abstract	48
4.2 Introduction	49

CHAPTER	PAGE
4.3	Experimental Parts 51
4.4	Results and Discussion 55
4.5	Conclusions 61
4.6	Acknowledgements 62
4.7	References 62
V	MECHANICAL, RHEOLOGICAL, AND SWELLING BEHAVIORS OF NATURAL RUBBER/ MONTMORILLONITE AEROGEL COMPOSITES PRODUCED BY FREEZE-DRYING
5.1	Abstract 78
5.2	Introduction 79
5.3	Experimental Parts 80
5.4	Results and Discussion 83
5.5	Conclusions 93
5.6	Acknowledgements 94
5.7	References 94
VI	SOLUTION CROSS-LINKED NATURAL RUBBER (NR)/ CLAY AEROGEL COMPOSITES: EMPHASIS ON THE CROSS-LINKING CONDITONS AND POLYMER CONCENTRATION
6.1	Abstract 113
6.2	Introduction 114
6.3	Experimental Parts 116
6.4	Results and Discussion 119
6.5	Conclusions 127
6.6	Acknowledgement 128
6.7	References 128

CHAPTER	PAGE
VII ELECTROLYTIC ADMICELLAR POLYMERIZATION OF PYRROLE ON NATURAL RUBBER/CLAY NANOCOMPOSITES	142
7.1 Abstract	142
7.2 Introduction	143
7.3 Experimental Parts	145
7.4 Results and Discussion	149
7.5 Conclusions	160
7.6 Acknowledgements	160
7.7 References	161
VIII FABRICATION AND CHARACTERIZATION OF NEW SEMICONDUCTING NANOMATERIALS COMPOSED OF NATURAL LAYERED SILICATES, NATURAL RUBBER, AND POLYPYRROLE	173
8.1 Abstract	174
8.2 Introduction	174
8.3 Experimental Parts	176
8.4 Results and Discussion	180
8.5 Conclusions	191
8.6 Acknowledgements	193
8.7 References	193
IX CONCLUSIONS AND RECOMMENDATIONS	215
REFERENCES	219
APPENDICES	225

CHAPTER	PAGE
Appendix A Preparation of Solution Cross-linked NR/ Clay Aerogel Composite	225
Appendix B Fabrication of New Semiconducting Nanomaterials	228
Appendix C Calculation of the Volume Conductivity	231
CURRICULUM VITAE	236

LIST OF TABLES

TABLE		PAGE
CHAPTER II		
2.1	Comparison between the critical concentration for forming the stable structure	9
2.2	Aerogels electrical conductivity	14
CHAPTER III		
3.1	Formulation of the rubber compound	37
CHAPTER IV		
4.1	Formulation of the rubber compound	66
4.2	Viscosity measurement of different rubber compounds	66
4.3	Curing characteristics of NR and its composites	67
4.4	Swelling ratios and calculated crosslink densities (v_c) of the thermal-and microwave-cured vulcanizates	68
4.5	Heat of reaction (ΔH) of partially-cured vulcanizates involving further vulcanization reaction	68
4.6	Elemental analysis of Na-MMT	69
4.7	Elemental analysis of NR/3MMT	69
CHAPTER V		
5.1	Formulation of compounding ingredients	98
5.2	Vulcanization characteristics, kinetic parameters, and activation energies of PNR and the corresponding composites obtained from ODR data	99

TABLE	PAGE
5.3 Crosslink density (V_e), equilibrium toluene uptake, and thermodynamic parameters of PNR and the corresponding composites	100
5.4 Diffusion coefficient and transport properties of PNR and the corresponding composites	100
5.5 Compression, density, and void volume fraction measurements of the studied materials	101
CHAPTER VI	
6.1 The estimated amount of the cross-linker (S_2Cl_2) in contact with 1 g of 2.5 wt% NR aerogels	130
6.2 EDX spectroscopy results of the 2.5 wt% NR aerogels formed at $T_{prep} = -18^\circ C$ under various S_2Cl_2 concentrations	130
6.3 The estimated amount of the cross-linker (S_2Cl_2) in contact with 1 g of the NR aerogels	131
6.4 Thermal characteristics of the studied materials	132
6.5 Theoretical and actual values of the organic matter in the dried composites	133
CHAPTER VII	
7.1 Electrochemical polymerization data of NR/PPy and a series of the nanocomposites	163
7.2 Elemental analysis of Na-MMT	163
7.3 Summary of the decomposition processes for unfilled NR/PPy and the nanocomposites	164
7.4 Weight percentage of NR/PPy and its nanocomposites remaining at $550^\circ C$	165

TABLE		PAGE
7.5	Mechanical properties of pure NR, NR/PPy, and the series of nanocomposites	165
CHAPTER VIII		
8.1	X-ray scattering data of Na ⁺ -MMT and nanocomposites	197
8.2	Dynamic mechanical properties of NPx and the corresponding nanocomposites	198
8.3	Summary of the thermal characteristics of the studied materials	199

LIST OF FIGURES

FIGURE	PAGE
CHAPTER II	
2.1	The crystal structure of the Na ⁺ -MMT. 3
2.2	Modes of particle association in clay suspensions: (a) dispersed; (b) face-to-face FF; (c) edge-to-face EF; and (d) edge-to-edge EE. 6
2.3	(A) Stable gel; (B) Nucleation at the edge of the vial; (C) Ice growth toward the center of vial; (D) Frozen solution; (E) After sublimation. 8
2.4	SEM micrograph of the clay aerogel. 8
2.5	The growth of ice crystals as a function of molecular weight of the polymer: (A, B) low molecular weight; (C, D) high molecular weight. SEM images of polymer/clay aerogel composites: (E) lamellar structure; (F) disordered structure. 11
2.6	(A) Randomly nucleated; (B) Cryostructured structures. 12
2.7	SEM micrographs of the fired clay aerogel: (A) at 850°C for 1 hr; (B) 900°C for 1 hr; (C) 900°C for 3 hr. 14
2.8	Scheme of different types of composite arising from the interaction between layered silicates and polymer matrices. 20
2.9	Chemical oxidative polymerization of pyrrole with FeCl ₃ . 24
2.10	The formation of polarons and bipolarons upon doping the PPy backbone. 24
2.11	Electrochemical polymerization of pyrrole. 27
2.12	Types of surfactant aggregates. 30
2.13	Typical adsorption isotherm of surfactants on a solid surface. 32
2.14	Schematic illustration of the admicellar polymerization process. 34

FIGURE	PAGE
CHAPTER IV	
4.1 Photographs of NR/clay aerogel nanocomposites: (a) NR/1MMT and (b) NR/2MMT.	70
4.2 XRD patterns of Na-MMT and Na-MMT aerogel.	71
4.3 XRD patterns of (a) NR/1MMT, (b) NR/2MMT, and (c) NR/3MMT nanocomposites.	71
4.4 SEM micrographs of (a) Na-MMT, (b) Na-MMT aerogel structure, and (c) the void inside the Na-MMT aerogel after the sublimation of ice.	72
4.5 SEM micrographs of (a) NR, (b) NR/1MMT, (c) NR/2MMT, (d) NR/3MMT, and (e) NR/3MMT at higher magnification.	73
4.6 Hardness results of freeze-dried NR and nanocomposites.	74
4.7 DSC thermograms of uncured (a) NR, (b) NR/1MMT, (c) NR/2MMT, and (d) NR/3MMT.	74
4.8 DSC thermograms of NR and its nanocomposites after microwave curing.	75
4.9 DSC thermograms of NR and its nanocomposites after thermal curing.	75
4.10 TGA results of NR and its nanocomposites.	76
4.11 The UV/vis absorbance spectra of a 1 wt% clay aqueous suspension in (a) distilled water and (b) 0.4M H ₂ SO ₄ .	76
4.12 Physical comparison between (a) starting clay solution and (b) clay solution after testing with benzidine.	77
4.13 Mechanism of thermal degradation of NR in the presence of ferric ion.	77

FIGURE	PAGE
CHAPTER V	
5.1 XRD patterns of the Na ⁺ -MMT and the corresponding composites.	102
5.2 SEM micrographs of (a) Na ⁺ -MMT aerogel, (b) PNR, (c) PNR/M1 composite, (d) PNR/M5 composite, and (e) PNR/M7 composite.	103
5.3 Schematic representation of the structure of Na ⁺ -MMT aerogel/PNR composites.	104
5.4 Rheographic curves of the neat PNR and the corresponding composites at 150°C.	105
5.5 (a) Plot of $\ln(D_{\max}-D_t)$ versus time and (b) Arrhenius plot between $\ln K$ versus $1000/T$ for the neat PNR and the corresponding composites.	106
5.6 Plots of (a) Q_t against $t^{1/2}$ and (b) $\log(Q_t/Q_\infty)$ against $\log t$ for the neat PNR and the corresponding composites in toluene at room temperature.	107
5.7 Stress–strain curves of the neat PNR and the corresponding composites.	108
5.8 Temperature dependence of (a) storage modulus, E' , and (b) loss tangent, $\tan \delta$, for the neat PNR and the corresponding composites.	109
5.9 Comparison amongst experimentally measured dynamic modulus at room temperature and theoretical predictions by introducing MRF.	110
5.10 Strain sweep measurements of the neat PNR and the corresponding composites at 150°C.	111

FIGURE	PAGE
5.11 Frequency dependence of (a) dynamic complex viscosity, η^* , and (b) dynamic storage modulus, G' , and loss modulus, G'' , of the neat PNR and the corresponding composites at 150°C.	112
CHAPTER VI	
6.1 (A) The equilibrium weight q_w (circles) and volume q_v (triangles) swelling ratios of the 2.5 wt% NR aerogels in toluene shown as a function of S_2Cl_2 concentration. $T_{prep} = 18^\circ C$ (filled symbols) and $-18^\circ C$ (open symbols). (B) The total volume of pores (V_p) in 2.5 wt% NR aerogels estimated from the uptake of methanol shown as a function of S_2Cl_2 concentration. $T_{prep} = 18^\circ C$ (filled symbols) and $-18^\circ C$ (open symbols).	134
6.2 (A) Typical stress–strain curves of the 2.5 wt% NR aerogels cross-linked at various S_2Cl_2 concentrations. $T_{prep} = -18^\circ C$. (B) Changes in the compressive modulus (filled symbols) and toughness at 30% strain (open symbols) of the 2.5 wt% NR aerogels prepared at various S_2Cl_2 concentrations. $T_{prep} = -18^\circ C$. (C) Density of the 2.5 wt% NR aerogels shown as a function of the S_2Cl_2 concentration. $T_{prep} = -18^\circ C$. (D) Comparison of the stress–strain curves of the 2.5 wt% NR aerogels formed at different temperatures. $S_2Cl_2 = 1\%$ (v/v).	135
6.3 Variation of the degree of cross-link (V_c) of the 2.5 wt% NR aerogels as a function of S_2Cl_2 concentration. $T_{prep} = -18^\circ C$.	136
6.4 SEM images of the 2.5 wt% NR aerogels cross-linked at different levels of S_2Cl_2 : (A) the neat control; (B) 0.25% (v/v); (C) 0.5%; (D) 1% (v/v); (E) 5% (v/v). $T_{prep} = -18^\circ C$.	136

FIGURE	PAGE
6.5 The bulk densities of NR aerogels before (filled symbols) and after the cross-linking reaction (open symbols) shown as a function of NR concentration. $T_{\text{prep}} = -18^{\circ}\text{C}$. $\text{S}_2\text{Cl}_2 = 1\%$ (v/v).	137
6.6 (A) Typical stress–strain curves of the neat and cross-linked NR aerogels, containing different weight fractions of NR, as indicated. (B, C) Compressive modulus (circles) and toughness at 30% strain (triangles) of the neat and cross-linked NR aerogels plotted as a function of NR concentration. $T_{\text{prep}} = -18^{\circ}\text{C}$. $\text{S}_2\text{Cl}_2 = 1\%$ (v/v).	138
6.7 (A) The equilibrium weight q_w (circles) and volume q_v (triangles) swelling ratios of the neat (filled symbols) and cross-linked (open symbols) NR aerogels in toluene shown as a function of NR concentration. $T_{\text{prep}} = -18^{\circ}\text{C}$. $\text{S}_2\text{Cl}_2 = 1\%$ (v/v). (B) The total volume of pores (V_p) in the neat and cross-linked NR aerogels estimated from the uptake of methanol shown as a function of NR concentration. $T_{\text{prep}} = -18^{\circ}\text{C}$. $\text{S}_2\text{Cl}_2 = 1\%$ (v/v). (C) Variation of the degree of cross-link (V_e) of the NR aerogels as a function of NR concentration. $T_{\text{prep}} = -18^{\circ}\text{C}$. $\text{S}_2\text{Cl}_2 = 1\%$ (v/v).	139
6.8 SEM micrographs of the 5 and 10 wt% NR aerogels: (A, B) before being cross-linked; (C, D) after being cross-linked. $T_{\text{prep}} = -18^{\circ}\text{C}$ and $\text{S}_2\text{Cl}_2 = 1\%$ (v/v).	140
6.9 Elemental mapping of the 10 wt% NR aerogel cross-linked at 1% (v/v) of S_2Cl_2 and T_{prep} of -18°C .	140
6.10 (A) TGA and (B) DTG thermograms of the neat and cross-linked NR aerogels, comprising various NR concentrations. $T_{\text{prep}} = -18^{\circ}\text{C}$ and $\text{S}_2\text{Cl}_2 = 1\%$ (v/v).	141

FIGURE	PAGE
CHAPTER VII	
7.1 FTIR spectra of (a) pure PPy and NR/PPy; and (b) NR/PPy and the nanocomposites.	166
7.2 XRD patterns of Na-MMT and the series of nanocomposites.	167
7.3 TEM photographs of (a) a 1 wt% clay suspension; (b) NR particles; (c) NR/PPy; and the nanocomposites containing (d) 1 phr; (e) 3 phr; (f) 5 phr; (g) 7 phr-MMT loading; and, (h) an ultrathin section of 7 phr-MMT loading.	168
7.4 Schematic of the structure of electropolymerized nanocomposites.	169
7.5 SEM micrographs of (a) NR/PPy; and the nanocomposites containing (b) 1 phr; (c) 3 phr; (d) 5 phr; and, (e) 7 phr-MMT loading at the same magnification ($\times 3500$).	170
7.6 Electrical conductivity of NR/PPy and the series of nanocomposites.	170
7.7 TGA curves of pure NR, PPy, and NR/PPy composite.	171
7.8 (a) TGA curves; and, (b) DTG curves of pure NR, NR/PPy and the series of nanocomposites.	172
CHAPTER VIII	
8.1 TEM images of the resulting materials: (a), (b), and (c) are micrographs of the NP ₁₀₀ , NP ₂₀₀ , and NP ₈₀₀ composites, respectively; (d), (e), and (f) are micrographs of the NP ₁₀₀ M ₇ , NP ₂₀₀ M ₇ , and NP ₈₀₀ M ₇ samples, respectively; (g), (h), and (i) are micrographs of an ultra thin section of the NP ₁₀₀ M ₇ , NP ₂₀₀ M ₇ , and NP ₈₀₀ M ₇ samples, respectively.	201

FIGURE	PAGE
8.2 SEM micrographs of (a) NP100, (c) NP200, and (e) NP800, with the corresponding nanocomposites (b) NP100M7, (d) NP200M7, and (f) NP800M7 at the same magnification ($\times 3500$).	203
8.3 Schematic of the formation mechanism of admicelled rubbers (path a) and the nanocomposites (path b).	204
8.4 XRD patterns of (a) Na^+ -MMT and $\text{NP}_{200}\text{M}_y$ series, and (b) Na^+ -MMT and NP_xM_7 nanocomposites.	205
8.5 Variation of polymerization rate of the nanocomposites with the clay loading.	206
8.6 FTIR spectra of (a) PPy and NP_x composites, and (b) NP_x and NP_xM_7 nanocomposites.	207
8.7 Electrostatic interaction between a protonated PPy chain and the clay layer.	208
8.8 Plot of the DC conductivity against clay loading of the nanocomposites.	208
8.9 Typical stress–strain curves of (a) pure NR and NP_x composites, and (b) NP_{200} and $\text{NP}_{200}\text{M}_y$ series.	209
8.10 Dependence of the mechanical properties of the $\text{NP}_{100}\text{M}_y$, $\text{NP}_{200}\text{M}_y$, and $\text{NP}_{800}\text{M}_y$ series on clay loading: (a) hardness, (b) tensile strength, (c) Young's modulus, and (d) elongation at break.	210
8.11 Temperature dependence of the (a) storage modulus, (b) loss modulus, and (c) loss tangent of NP_x and the corresponding nanocomposites.	211
8.12 TGA curves of (a) pure NR, PPy, and NP_x composites, and (b) NP_x and NP_xM_7 nanocomposites.	212
8.13 DTG curves of pure NR, NP_x , and NP_xM_7 nanocomposites.	213

FIGURE		PAGE
8.14	Plots of $\ln\left\{\ln\left[\frac{W_0 - W_f}{W_t - W_f}\right]\right\}$ against θ .	214
8.15	Variation of the calculated activation energy of the nanocomposites with clay loading.	214

ABBREVIATIONS

APS	Ammonium Persulfate
AOT	Sodium Bis(2-ethylhexyl) Sulfosuccinate
CAC	Critical Admicelle Concentration
CB	Carbon Black
CEC	Cation Exchange Capacity
CMC	Critical Micelle Concentration
CNTs	Carbon Nanotubes
CPs	Electrically Conducting Polymers
CR	Chloroprene Rubber
CV	Conventional Vulcanization System
DBSA	Dodecyl Benzene Sulfonic Acid
DI	Deionized Water
DMA	Dynamic Mechanical Analysis
DSC	Differential Scanning Calorimetry
DTG	Derivative Thermogravimetry
EDX	Energy Dispersive X-Ray Spectroscopy
EE	Edge to Edge Association
EF	Edge to Face Association
ER	Electrorheological
EV	Efficient Vulcanization System
FF	Face to Face Association
G	Gibb Free Energy
H	Enthalpy
HATR-FTIR	Horizontal Attenuated Total Reflection-Fourier Transform Infrared Spectroscopy
HCl	Hydrochloric Acid
ITO	Indium-Tin Oxide
LCST	Lower Critical Solution Temperature
LDH	Layered Double Hydroxide

LDPE	Low Density Polyethylene
LEDs	Light Emitting Diodes
MRF	Modulus Reduction Factor
MW	Molecular Weight
Na ⁺ -MMT	Sodium Montmorillonite
NR	Natural Rubber
OMCAS	Organically Modified Clay Aerogels
OMLS	Organically Modified Layered Silicates
PAA	Poly(acrylic acid)
PANI	Polyaniline
PHB	Poly[(<i>R</i>)-3-hydroxybutyrate]
PHR	Parts Per Hundred of Rubber
PIB	Butyl Rubber
PNIPAM	Poly (<i>N</i> -isopropyl acrylamide)
PNR	Prevulcanized Natural Rubber
POSS	Polyhedral Oligomeric Silsesquioxane
PPy	Polypyrrole
PS	Polystyrene
PS-PEGMA	Polystyrene-Poly(ethylene glycol) Monomethacrylate
PVOH	Poly(vinyl alcohol)
PZC	Point of Zero Charge
S	Conformational Entropy
SDS	Dodecyl Sulfate Sodium Salt
SEM	Scanning Electron Microscopy
SWCNT	Single-Walled Carbon Nanotubes
TEM	Transmission Electron Microscopy
TGA	Thermogravimetric Analysis
TMTD	Tetramethylthiuram Disulfide
TN	Titanate Nanowire
XNBR	Carboxylated Nitrile Rubber
XRD	X-Ray Diffraction

XRF	X-Ray Fluorescence Spectrometer
ZDEC	Zinc Diethyl Dithiocarbamate
ZnO	Zinc Oxide

LIST OF SYMBOLS

T_g	Glass Transition Temperature
T_{prep}	Preparation Temperature
n_1'	Number of Mole of Adsorbed Surfactant/Gram of Solid Adsorbent at Equilibrium
$\Delta C'$	Molar Concentration Difference of Surfactant Before and After Equilibrium Adsorption in Liquid Phase
m	Mass of the Adsorbent
V	Volume of Liquid Phase
Γ_1	Surface Concentration of the Surfactant
a_s	Surface Area per Unit Mass of the Adsorbent
a_1^s	Surface Area per Adsorbate Molecule
N	Avogadro's Number
$\dot{\gamma}$	Shear Rate
ω	Angular Velocity
R_c	Container Radius
R_b	Spindle Radius
χ	Container Radius
η	Viscosity
τ	Shear Stress
λ	X-Ray Wavelength
d_{001}	Interlayer Spacing
θ	Diffraction Angle
M_c	Average Molecular Weight between the Network Crosslinks
V_c	Cross-Link Density
V_r	Volume Fraction of Rubber in a Swollen Network
V_1	Molar Volume of Toluene
χ_1	Flory-Huggins Interaction Parameter
W_d	Weight of Dry Rubber

W_s	Weight of Solvent Adsorbed by the Sample
f_{ins}	Weight Fraction of Fillers
ρ_d	Density of Rubber
ρ_s	Density of Toluene
$n_{S_2Cl_2}$	Number of Moles of S_2Cl_2
$d_{S_2Cl_2}$	Density of S_2Cl_2
$MM_{S_2Cl_2}$	Molar Mass of S_2Cl_2
q_b	Amount of Benzene Absorbed by 1 Gram of NR Aerogels
m_b	Weight of Swollen NR Aerogels in Benzene
$K(T)$	Specific Rate Constant
K_0	Constant
T	Temperature
t	Time
R	Universal Gas Constant
E_a	Apparent Activation Energy
Q_t	Toluene Adsorption
Q_∞	Equilibrium Swelling Ratio
D	Diffusion Coefficient
h	Sample Thickness
k	Constant
n	Transport Mechanism
q_w	Equilibrium Weight Swelling Ratio
q_v	Equilibrium Volume Swelling Ratio
m_{tot}	Weight of the Equilibrium Swollen NR Aerogels
m_{dry}	Weight of the Dry NR Aerogels
D_{tot}	Diameter of the Equilibrium Swollen NR Aerogels
D_{dry}	Diameter of the Dry NR Aerogels
V_p	Pore Volume of the Network
m_M	Weight of the NR Aerogels Immersed in Methanol
d_M	Density of Methanol
σ_{dk}	Volume Conductivity

ρ_v	Volume Resistivity
V	Voltage
I	Current
R	Resistance
T_c	Vulcanization Temperature
t_{S_2}	Scorch Time
t_{90}	Optimum Cure Time
S_{\max}	Maximum Rheometric Torque
S_{\min}	Minimum Rheometric Torque
ΔS	Torque Difference
ΔH	Heat of Vulcanization
E'	Dynamic Storage Modulus
E	Tensile Modulus of Matrix
E_m	Tensile Modulus of Composite
E_f	Young's Modulus of Na ⁺ -MMT
α	Aspect Ratio
φ	Volume Fraction of Na ⁺ -MMT
ξ	Constant
G'	Storage Modulus (Dynamic Rheometer)
G''	Loss Modulus
η^*	Complex Viscosity
T_0	Onset Decomposition Temperature
T_d	Peak Decomposition Temperature
T_s	Reference Temperature
dW/dT	Rate of Weight Loss
W_0	Initial Weight of Sample
W_f	Final Weight of Sample
W_t	Weight of Sample at time t